Activation and Ripening of Impregnated Manganese Containing Perovskite SOFC Electrodes under Redox Cycling

G. Corre,[†] G. Kim,[‡,§] M. Cassidy,[†] J. M. Vohs,[‡] R. J. Gorte,[‡] and J. T. S. Irvine*[,†]

School of Chemistry, University of St. Andrews, Fife KY16 9ST, U.K., Department of Chemical and Biomolecular Engineering, University of Pennsylvania, Philadelphia, Pennsylvania 19104, and Ulsan National Institute of Science and Technology (UNIST), 194, Banyeon, Ulsan 689-805, South Korea

Received November 19, 2008. Revised Manuscript Received January 16, 2009

The impregnation of electrode precursor solutions is a very powerful technique for creating novel electrode microstructures constrained within preformed scaffolds. Here we report on the microstructural evolution of Mn-containing perovskites impregnated into yttria stabilized zirconia scaffolds on heating and redox cycling. Good performances have previously been reported for SOFC anodes with similar structure, and our objective is to better understand the origins of this good performance. For $La_{0.75}Sr_{0.25}Cr_{0.5}Mn_{0.5}O_{3-\delta}$ a remarkable thin coating with microfissures is formed on the scaffold after firing the electrode precursors at 1200 °C, and such behavior can be considered as wetting of one oxide by another. On further treating this microstructure at 800 °C in H_2 the microstructure changes dramatically forming an interconnected array of ~10 nm scale particles. This seems to offer a very attractive structure with extensive triple phase boundary regions where electrochemical reactions can occur. On reoxidation at this temperature the particles reagglomerate to form a structure approaching the initial smooth coating. Performing similar procedures on the system $La_{0.33}Sr_{0.67}Ti_xMn_{1-x}O_{3\pm\delta}$, we find that the wetting only occurs if Mn is present in the oxide and that the degree of wetting increases with Mn concentration. This favorable interaction between the Mn containing perovskites and the zirconia scaffold must be associated with a chemical interaction between impregnated oxide and substrate. The strength of this interaction decreases on reduction allowing the perovskite electrode to form nanoscale particles which along with appropriate additional catalysts provide good electrode functionality.

Introduction

Solid oxide fuel cells (SOFCs) are very promising electrochemical devices that convert chemical energy directly to electricity.[1] Besides their attractive high electrical conversion efficiency, they offer many advantages over conventional means of electricity production, such as scalability, low emissions, low noise, and quality of power. Performance is already good, but important issues to be addressed before this technology can be fully implemented relate to durability, system cost, and fuel flexibility. Critical to this development are the structures of the electrode/electrolyte interfaces, which need to be controlled at the nano- and microscales to optimize gas transfer, electronic and ionic conduction, and catalytic activity. Here we describe some quite remarkable morphological changes that occur on thermal processing and redox cycling of some impregnated perovskite electrodes, which are of interest as possible SOFC anodes.

The present standard SOFC anode is a cermet made of Ni and YSZ (yttria stabilized zirconia). While offering high catalytic activity for hydrogen oxidation, Ni/YSZ cermets show several limitations. The use of hydrocarbons is limited due to the Ni activity for coking, especially for higher hydrocarbons or even methane under low steam conditions.[2] Other issues relate to sulfur and other impurity tolerance and to degradation due to oxidation at high utilization or shut down conditions. This has led to considerable efforts in developing alternative anode materials to Ni/YSZ cermets. The main properties targeted are high mixed ionic/electronic conductivity, stability to redox cycles, and limited activity for carbon formation when fuelled with hydrocarbons.[3]

Regardless of the materials involved in a SOFC anode, the microstructure is a key factor to achieve high performance.[4] An ideal microstructure would offer the highest triple phase boundary (TPB) length for electrochemical reactions and an optimized contact between the electrolyte and the anode and be stable during operation. The relation between microstructure and performances has been addressed in several publications mainly for Ni/YSZ cermets.[5−12] The

[†] University of St. Andrews.
[‡] University of Pennsylvania.
[§] Ulsan National Institute of Science and Technology.

(1) Minh, N. Q. *J. Am. Ceram. Soc.* **1993**, *76*, 563.
(2) Toebes, M. L.; Bitter, J. H.; van Dillen, A. J.; de Jong, K. P. *Catal. Today* **2002**, *76*, 33.
(3) Atkinson, A.; Barnett, S.; Gorte, R. J.; Irvine, J. T. S.; McEvoy, A. J.; Mogensen, M. B.; Singhal, S.; Vohs, J. *Nat. Mater.* **2004**, *3*, 17.
(4) Jiang, S. P.; Chan, S. H. *J. Mater. Sci.* **2004**, *39*, 4405.
(5) Primdahl, S.; Mogensen, M. *J. Electrochem. Soc.* **1997**, *144*, 3409.
(6) Brown, M.; Primdahl, S.; Mogensen, M. *J. Electrochem. Soc.* **2000**, *147*, 475.
(7) Virkar, A. V.; Chen, J.; Tanner, C. W.; Kim, J. W. *Solid State Ionics* **2000**, *131*, 189.
(8) Lee, J. H.; Moon, H.; Lee, H. W.; Kim, J.; Kim, J. D.; Yoon, K. H. *Solid State Ionics* **2002**, *148*, 15.
(9) Lee, J. H.; Heo, J. W.; Lee, D. S.; Kim, J.; Kim, G. H.; Lee, H. W.; Song, H. S.; Moon, J. H. *Solid State Ionics* **2003**, *158*, 225.
(10) Guo, W.; Liu, J. *Solid State Ionics* **2008**, *179*, 1516.

10.1021/cm803149v CCC: $40.75
Published on Web 02/11/2009

microstructure of a SOFC electrode is intimately linked to the method used for the anode fabrication. Normally cermet or oxide anodes are made by conventional ceramic processing techniques such as tape casting,[13,14] hot pressing,[15] or screen printing.[16] Such methods do not generally favor the creation of high surface area electrocatalysts due to the high temperatures employed. There has been significant activity in recent years seeking to develop alternative routes that provide enhanced catalytic activity. Of particular importance are the solution impregnation into preformed electrode scaffolds and in situ firing of catalysts such as ceria and Pd by Gorte et al.[17,18] Other approaches of note are the direct impregnation of nanoparticle electrocatalysts[19] and the in situ exolution of metallic nanoparticle electrocatalysts.[20]

Using the impregnation approach, we have recently reported high performances SOFC anodes able to operate on humidified (3% H_2O) hydrogen and methane gases.[21] Those anodes were prepared by aqueous infiltration of nitrate salts to produce 45 wt % $La_{0.75}Sr_{0.25}Cr_{0.5}Mn_{0.5}O_3$ (LSCM) in a 65% porous yttria-stabilized zirconia (YSZ) scaffold. To investigate the origins of these high performances, we have studied the evolution microstructure of LSCM impregnated YSZ composites. In this study, we investigate how the structure evolves in reducing conditions using SEM micrographs and conductivity measurements. The study has been extended to the $La_{0.33}Sr_{0.67}Ti_xMn_{1-x}O_{3\pm\delta}$ (LSTM) perovskite family to help to understand the phenomena occurring in such composites paying particular attention to the role of Mn content in controlling the interface. These Mn/Ti oxides have previously shown interesting activities as SOFC anodes as ceramic electrodes.[22,23]

Experimental Section

The composite electrode structures were prepared in a similar manner to that previously reported by the University of Pennsylvania group.[18] This method involves the preparation of a porous YSZ scaffold, followed by infiltration of the active components. The porous YSZ was prepared from the same slurries as those used in tape casting for the production of fuel cells. The slurries were prepared by mixing YSZ powder (Tosoh Corp., 8 mol % Y_2O_3-doped ZrO_2, 0.2 μm) with distilled water, a dispersant (1.27 g, Duramax 3005, Rohm & Haas), binders (10.2 g HA12 and 14.4 g B1000, Rohm & Haas), and graphite. Slabs (1 mm × 1 mm × 10 mm) prepared from this slurry were then fired to 1500 °C to produced a YSZ structure with a porosity of approximately 65%.

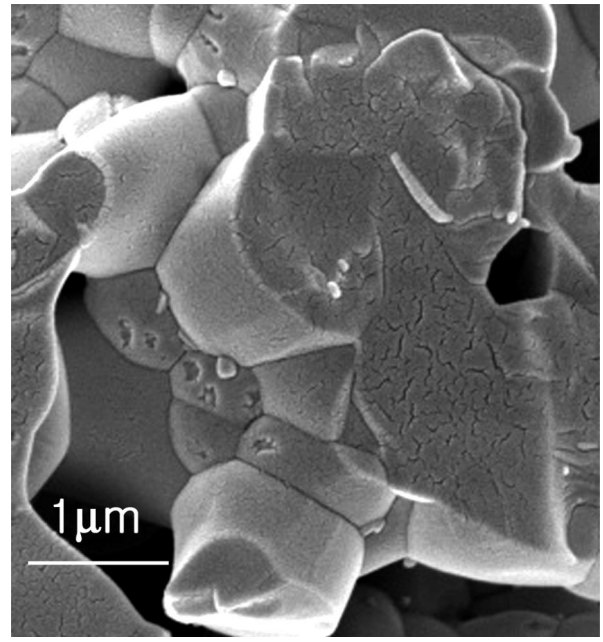

Figure 1. Coating of $La_{0.75}Sr_{0.25}Cr_{0.5}Mn_{0.5}O_3$ (LSCM) over YSZ scaffold prepared by solution impregnation and then firing at 1200 °C in air. Note the crazed texture within the LSCM coating on the YSZ scaffold offering a rich three phase boundary structure.

After synthesizing the YSZ scaffold, the desired perovskite was added at a loading of 45-wt % using an aqueous nitrate solution. For LSCM, the impregnating solution was prepared by adding $La(NO_3)_3 \cdot 6H_2O$ (Alfa Aesar, ACS 99.9%), $Sr(NO_3)_2$ (Alfa Aesar, ACS 99.0%), $Cr(NO_3)_3 \cdot 9H_2O$ (Alfa Aesar, ACS 98.5%), and $Mn(NO_3)_2 \cdot 4H_2O$ (Alfa Aesar, ACS 99.98%) to distilled water in the correct molar ratios, then mixing this with citric acid (99.5%, Aldrich) to produce a solution with a citric acid/metal-ion ratio of 2:1. For LSTM, the impregnating solution was prepared by using the same precursors for La, Sr, and Mn but using $(CH_3CH(O-)CO_2 \cdot NH_4)_2 \cdot Ti(OH)_2$ (dihydroxy-bis-ammonium, lactate, titanium(IV), Alfa Aesar) as a Ti precursor. No citric acid was added for LSTM solutions.

Infiltrating porous YSZ with such solutions is a multi-step process. After the porous layer has been infiltrated, the ceramic wafer is heated in air to 450 °C to decompose the nitrate ions and the citric acid. This procedure has to be repeated until the desired weight loading of oxide is achieved. Finally, when the required loading has been reached, the wafer is heated in air at high temperature (850−1300 °C) to form the perovskite phase. XRD was used in each case to verify that the correct phase had been formed within the scaffold.

The electronic conductivities of impregnated YSZ composites were measured as a function of temperature in air and in humidified H_2 using standard four-probe measurements. SEM images were taken on fractured fuel cells, after conditioning using a JEOL 5600 SEM.

Results

1. $La_{0.75}Sr_{0.25}Cr_{0.5}Mn_{0.5}O_3$ (LSCM). Early studies on porous YSZ structures impregnated with LSCM have

(11) de Boer, B.; Gonzalez, M.; Bouwmeester, H. J. M.; Verweij, H. *Solid State Ionics* **2000**, *127*, 269.
(12) Golbert, J.; Adjiman, C. S.; Brandon, N. P. *Ind. Eng. Chem. Res.* **2008**, *47*, 7693.
(13) Rietveld, G.; Nammensma, P.; Ouweltjes, J. P. *Solid Oxide Fuel Cells VII (SOFC VII)* **2001**, *16*, 125.
(14) Simner, S. P.; Stevenson, J. W.; Meinhardt, K. D.; Canfield, N. L. *Solid Oxide Fuel Cells VII (SOFC VII)* **2001**, *16*, 1051.
(15) Tietz, F.; Buchkremer, H. P.; Stover, D. *J. Electroceram.* **2006**, *2−4*, 701.
(16) Gardner, F. J.; Day, M. J.; Brandon, N. P.; Pashley, M. N.; Cassidy, M. *J. Power Sources* **2000**, *86*, 122.
(17) Gross, M. D.; Vohs, J. M.; Gorte, R. J. *Electrochem. Solid-State Lett.* **2007**, *10*, B65.
(18) Gross, M. D.; Vohs, J. M.; Gorte, R. J. *J. Electrochem. Soc.* **2007**, *154*, B694.
(19) Sholklapper, T. Z.; Radmilovic, V.; Jacobson, C. P.; Visco, S. J.; De Jonghe, L. C. *Electrochem. Solid-State Lett* **2007**, *10*, B74.
(20) Madsen, B. D.; Kobsiriphat, W.; Wang, Y.; Marks, L. D.; Barnett, S. A. *J. Power Sources* **2007**, *166*, 64.
(21) Kim, G.; Corre, G.; Irvine, J. T. S.; Vohs, J. M.; Gorte, R. J. *Electrochem. Solid-State Lett.* **2008**, *11*, B16.
(22) Ovalle, A.; Ruiz-Morales, J. C.; Canales-Vázquez, J.; Marrero-López, D.; Irvine, J. T. S. *Solid State Ionics* **2006**, *177*, 19.
(23) Ruiz-Morales, J. C.; Canales-Vázquez, J.; Savaniu, C.; Marrero-López, D.; Zhou, W.; Irvine, J. T. S. *Nature* **2006**, *439*, 568.

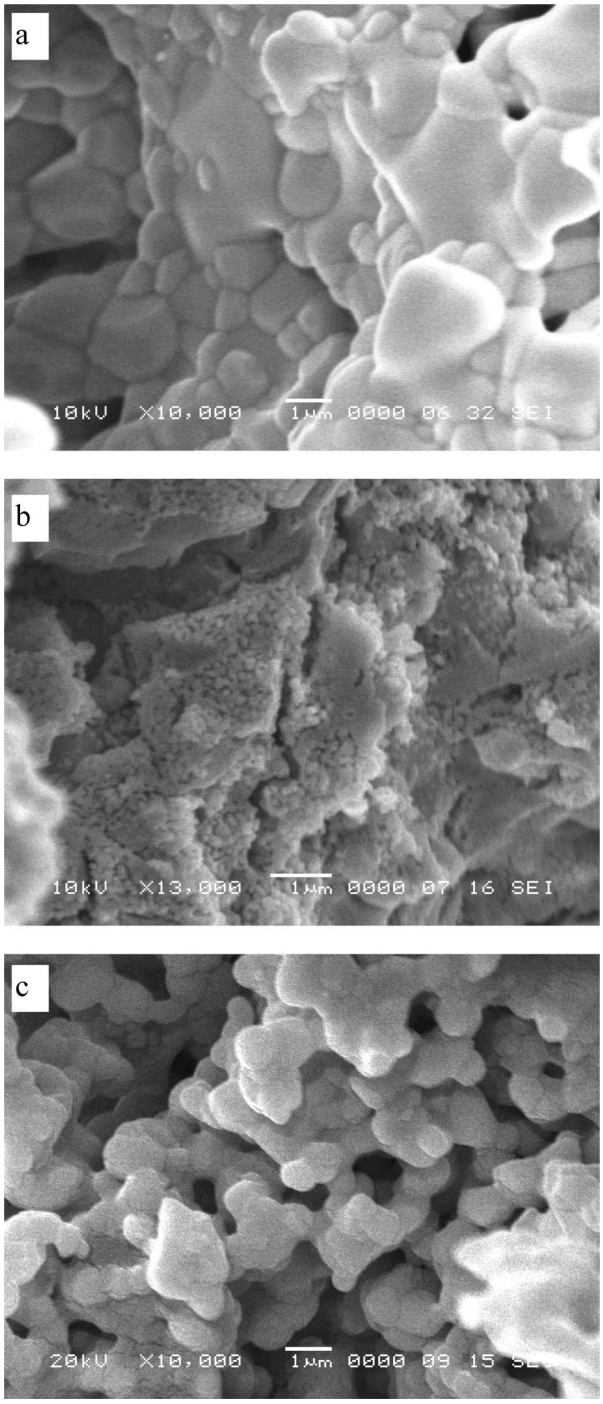

Figure 2. Scanning electron micrographs of LSCM-YSZ composites after reduction in humidified (3% H_2O) H_2 for 5 h at (a) 700 °C, (b) 800 °C, and (c) 900 °C.

demonstrated that the LSCM phase forms a coating over the YSZ surface after high temperature sintering in air,[21−24] Figure 1. Such a phenomenon has also been observed with $La_{0.8}Sr_{0.2}MnO_3$ (LSM) particles on YSZ single crystals,[25,26] where the minimization of the surface free energy caused LSM particles to spread over the YSZ crystal to form a dense

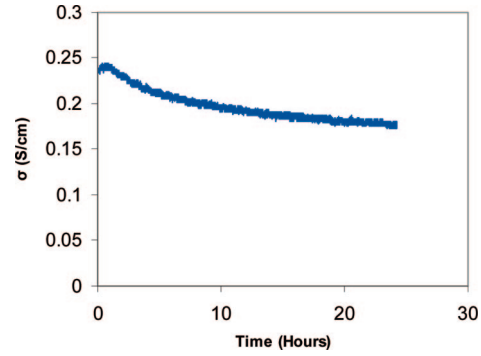

Figure 3. Evolution with time of the conductivity of a LSCM-YSZ composite at 800 °C in humidified (3% H_2O) H_2.

film upon calcination in air above approximately 1400 K. However, in previous studies of impregnated YSZ porous structures, such a coating of the YSZ by the impregnated oxide was not observed. Instead, the impregnated phase formed particles easily distinguishable from the YSZ scaffold for example, for impregnated ceria,[27] for impregnated LSF,[17] or for impregnated lanthanum strontium titanate, LST.[28] Therefore we may see two substantially different microstructures depending upon the nature of the impregnated phase. There is a strong analogy with the way a liquid would behave on a solid surface, by wetting this surface (LSCM, LSM) or forming a drop on this surface (LST).

The wetting of the YSZ electrode scaffold by a conductive oxide ensures a good connectivity for the electronic conductive phase and hence minimizes ohmic losses in the composite electrode. Such a uniform coating would restrict the three phase boundary length and hence would increase polarization resistances in such an anode. This would not be expected to give the good performance observed recently for LSCM impregnated zirconia scaffold electrodes; however, it should be noted that the microcracking in the coating, visible in Figure 1, may provide the required three-phase boundary length for efficient operation as an SOFC anode.

The assumption that the film microstructures produced at 1200 °C in air is relevant to fuel cell anode conditions is, however, incorrect as there is a complex and interesting evolution of the impregnated microstructure in a reducing environment. On annealing at 700 °C (Figure 2a), the structure remains close to that produced in air at 1200 °C, but on annealing at 800 °C (Figure 2b) the dense film breaks up into interconnected nanoscale particles covering the YSZ surface. Under fuel conditions, a nanoporous conductive coating layer is therefore formed on the YSZ surface, which ensures a really high triple phase boundary length for electrochemical reactions within the anode.[29] The increase in temperature from 700 to 800 °C seems to allow this change of structure to happen. At 700 °C, such a porous structure cannot be observed in the timescales studied, and the anode offers therefore a smaller TPB. At 900 °C (Figure 2c), LSCM crystal growth can be observed, leading to a different

(24) Kim, G.; Corre, G.; Irvine, J. T. S.; Vohs, J. M.; Gorte, R. J. *Electrochem. Solid-State Lett.* **2008**, *11*, B16.
(25) Huang, Y.; Vohs, J. M.; Gorte, R. J. *J. Electrochem. Soc.* **2005**, *152*, A1347.
(26) Huang, Y.; Vohs, J. M.; Gorte, R. J. *Electrochem. Solid-State Lett.* **2006**, *9*, A237.
(27) Gross, M. D.; Vohs, J. M.; Gorte, R. J. *Electrochem. Solid-State Lett.* **2007**, *10*, B65.
(28) Lee, S.; Kim, G.; Vohs, J. M.; Gorte, R. J. *J. Electrochem. Soc.* **2005**, *155*, A1179.
(29) Kim, G.; Lee, S.; Shin, J. Y.; Corre, G.; Irvine, J. T. S.; Vohs, J. M.; Gorte, R. J. *Electrochem. Solid-State Lett.* **2009**, *12*, B48.

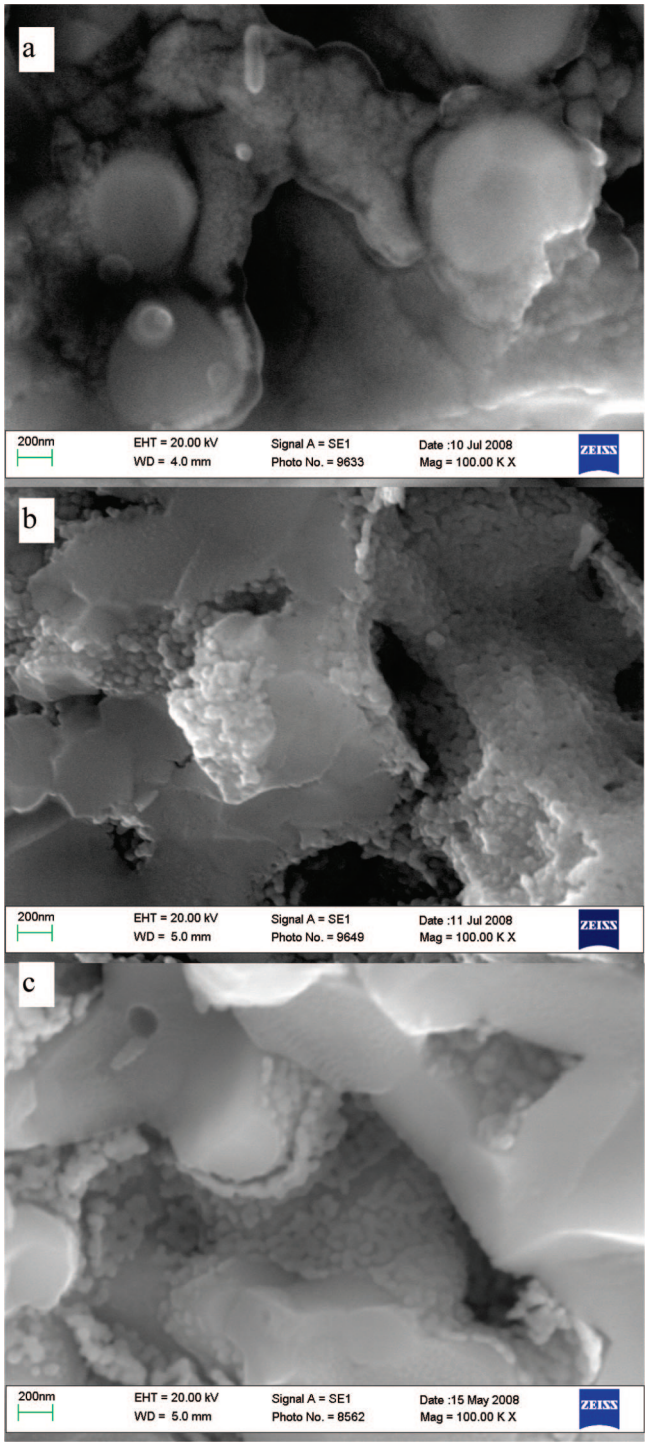

Figure 4. Scanning electron micrographs of LSCM-YSZ composites at different times of reduction in humidified (3%H_2O) H_2: (a) 1 h, (b) 3 h, and (c) 5 h.

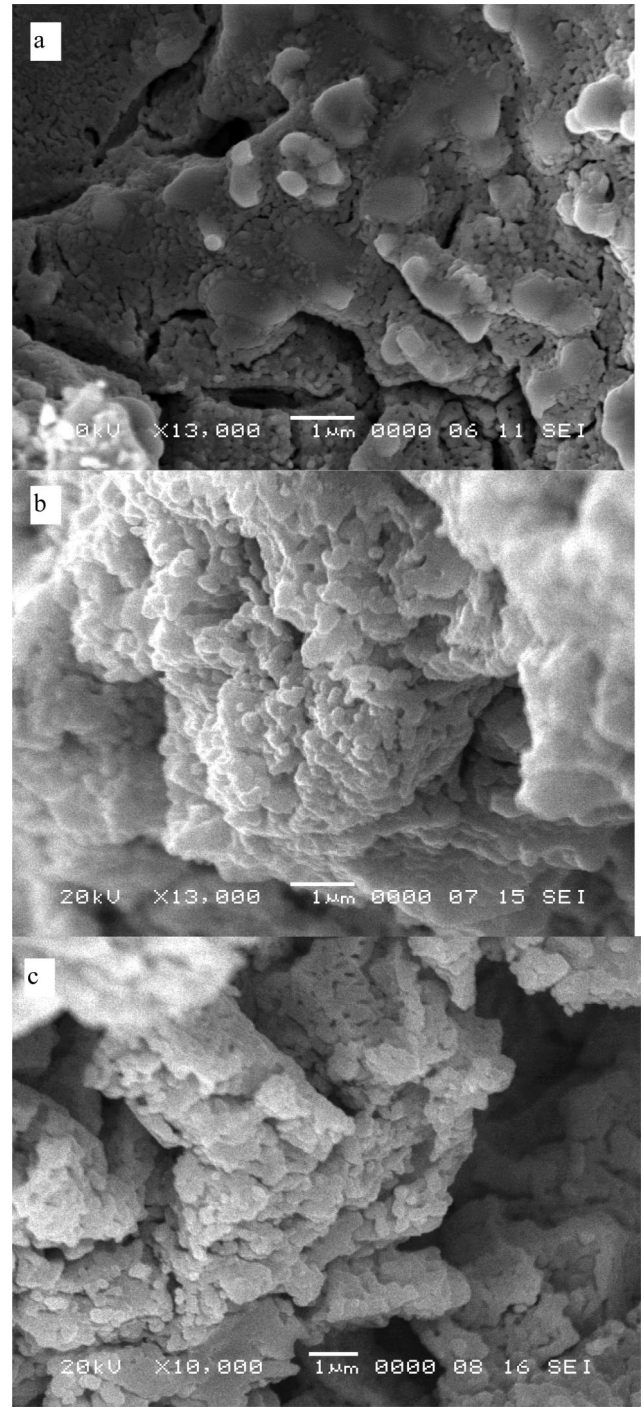

Figure 5. Scanning electron micrographs of LSCM-YSZ composites at different times of reoxidation: (a) 5 h, (b) 10 h, and (c) 20 h.

structure with larger grains, which shows similarities to previously published LSCM anodes prepared by methods such as combustion synthesis.[30]

Reported fuel cell performances on similar electrodes but containing a small amount of Pd and CeO_2 to enhance catalytic activity were very good. Performance in hydrogen improved on increasing temperature from 700 °C (560 mW/cm^2) to 800 °C (1.1 W/cm^2) to 900 °C (1.4 mW/cm^2).[21]

The evolution of the dense film toward a porous structure can be expected to influence the conductivity of these composites. Initial conductivities of LSCM impregnated YSZ structures have been reported before and are high enough for use as a functional layer in an SOFC anode.[21] Figure 3 shows the evolution of this conductivity with time for a sample that had been equilibrated at 700 °C then further heated and maintained at 800 °C in humidified (3% H_2O) H_2, that is, in fuel cell anodic conditions. The conductivity decreases continuously toward a stable value as the microstructure evolves. The greatest rate of this deterioration occurs within the first 24 h, and once completed, the conductivity has dropped by 28%. This microstructural

(30) Tao, S. W.; Irvine, J. T. S. *J. Electrochem. Soc.* **2004**, *151*, A252.

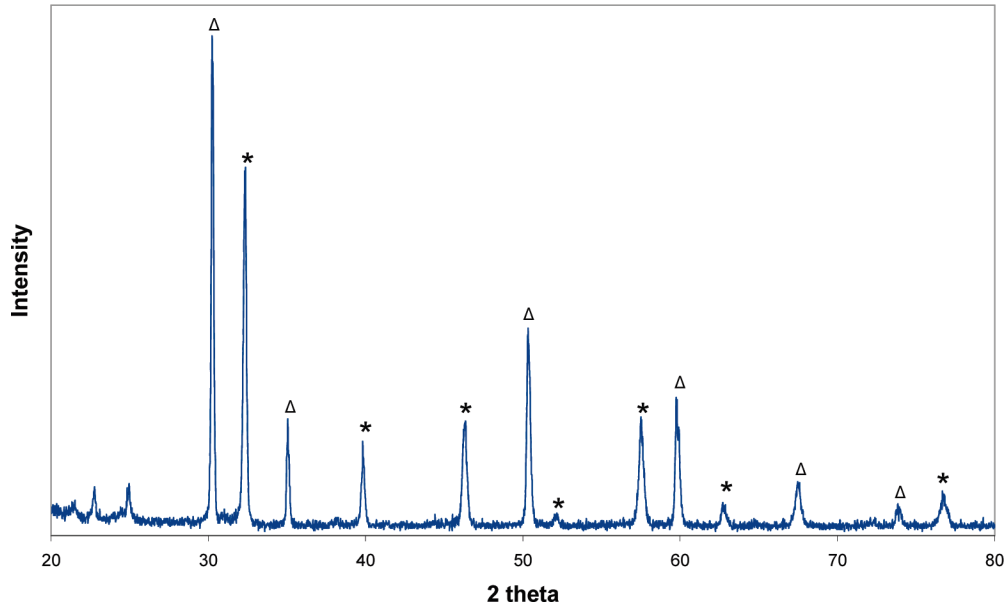

Figure 6. Typical XRD of a LSTM-YSZ composite with 30 wt % LSTM for $La_{0.33}Sr_{0.67}Ti_{0.67}Mn_{0.33}O_{3\pm\delta}$, formed by infiltration into porous YSZ: LSTM (*) and YSZ (△), peaks before 30° 2θ due to the XRD holder.

induced conductivity decrease can be better understood by analyzing SEM images of the structure taken after different times of reduction, as displayed in Figure 4. The original structure is a dense LSCM film covering the YSZ (Figures 1 and 2a) but after 1 h at 800 °C (Figure 4a), the beginning of a new structure can be seen with individual grains becoming apparent on the nanoscale. After 3 h (Figure 4b), the coating has a much more distinct granular type of morphology but it can be seen (upper right of the image) that there are still many necks between the particles and they are still very much interconnected and almost form a continuous layer. After 5 h (Figure 4c), the grains appear to be more distinct than on the previous images, and although still interconnected, many gaps become visible between the grains. This loss of interconnectivity with the LSCM phase explains the loss of conductivity as a function of time. Meanwhile, it is responsible for an increase in the surface area of the LSCM phase and in turn of the TPB length within the anode, making initial performances outstanding.

On reoxidation at 800 °C of a sample that had previously been reduced at this temperature, the transition from an even coating of LSCM to the nanoscale particulate structure is seen to be reversed. After 5 h of oxidation (Figure 5a) the nanoparticles are seen to have started to coalesce; after 10 and 20 h (Figure 5b,c) these particles are now fully merged, although the coating is not as smooth as initially observed after 1200 °C sinter.

Conductivities recorded on a LSCM/YSZ composite in humidified hydrogen after a full redox cycle show some irreversibility in the redox process. While the conductivity at 800 °C was initially measured to be 0.24 S cm^{-1}, after reduction, structural reorganization, and reoxidation at this temperature, the conductivity at 800 °C was only 0.15 S cm^{-1}. The conductivity is lower after a redox cycle as might be expected from the change in the nature of the coating.

2. $La_{0.33}Sr_{0.67}Ti_xMn_{1-x}O_{3\pm\delta}$ (LSTM). To investigate the role played by Mn in the wetting of YSZ, structures of LSTM with different Mn/Ti ratios impregnated into a YSZ backbones have been analyzed after high temperature firing. Figure 6 reports the diffraction pattern obtained for a typical LSTM composition after firing at 1200 °C, showing that the desired perovskite structure has been obtained in situ.

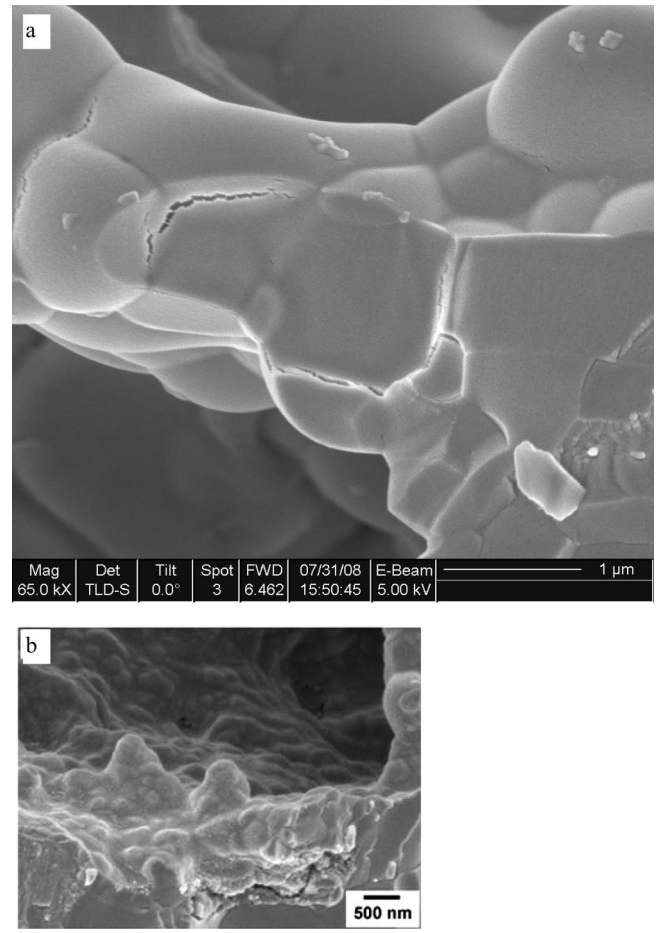

Figure 7. Scanning electron micrographs of (a) $La_{0.33}Sr_{0.67}Ti_{0.67}Mn_{0.33}O_{3\pm\delta}$−YSZ composite (Mn/Ti = 2) after sintering at 1200 °C and $La_{0.8}Sr_{0.2}TiO_3$−YSZ composite after sintering at 1200 °C.

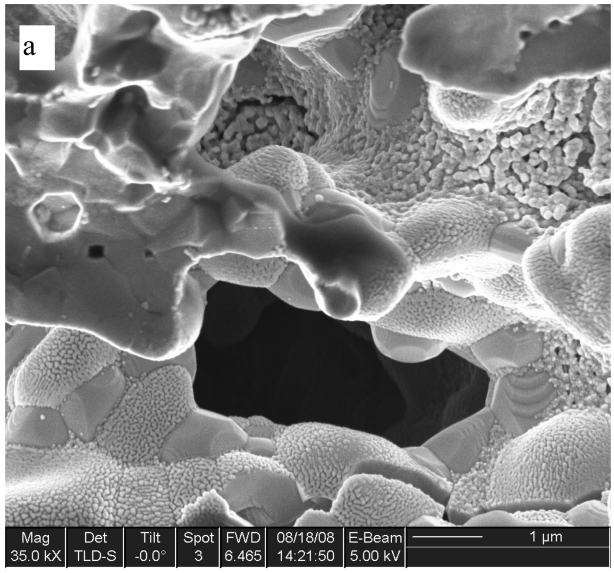

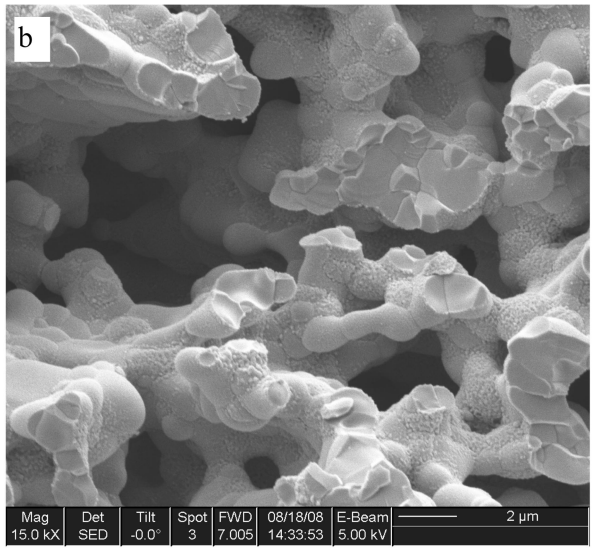

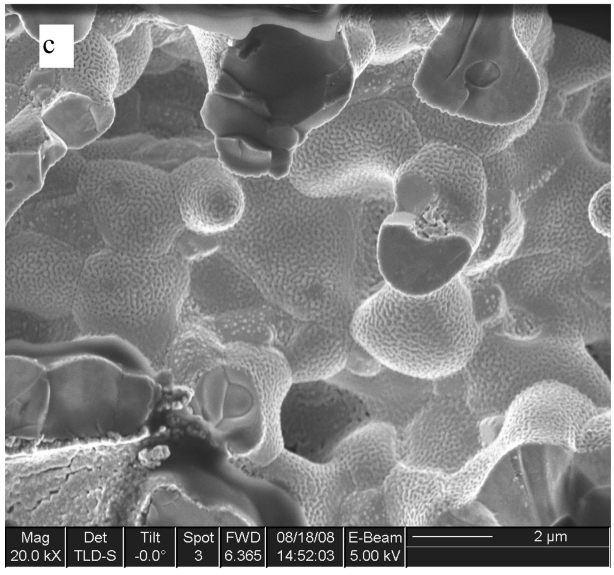

Figure 8. Scanning electron micrograph of LSTM-YSZ composites after reduction at 800 °C in humidified (3% H_2O) H_2 for several hours (a) Mn/Ti = 2 sintered at 1300 °C, (b) Mn/Ti = 1 sintered at 1200 °C, and (c) Mn/Ti = 0.5 sintered at 1300 °C.

Figure 7a shows a SEM image of the structure after high temperature firing for a $La_{0.33}Sr_{0.67}Ti_{0.67}Mn_{0.33}O_{3\pm\delta}$−YSZ composite (Ti/Mn = 2). This structure is similar to that observed for the higher manganese content $La_{0.33}Sr_{0.67}Ti_{0.5}Mn_{0.5}O_{3\pm\delta}$−YSZ (Ti/Mn = 1) and

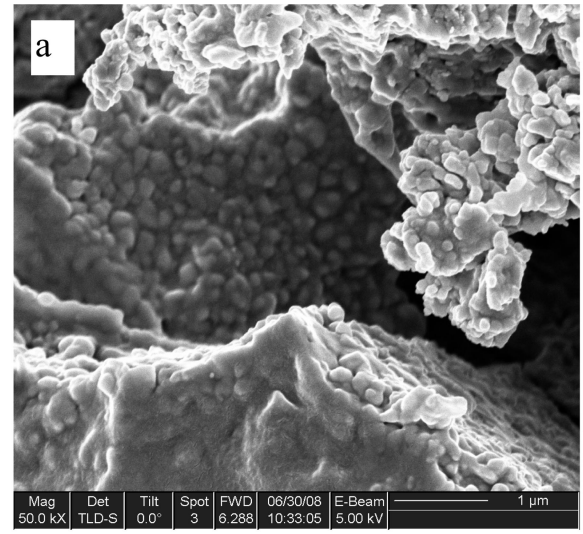

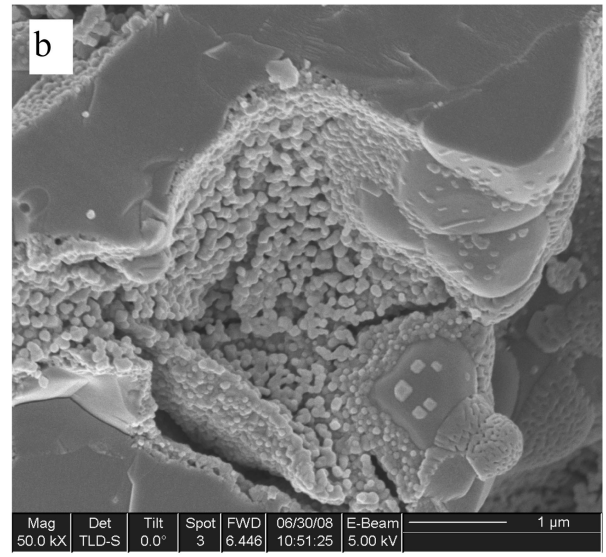

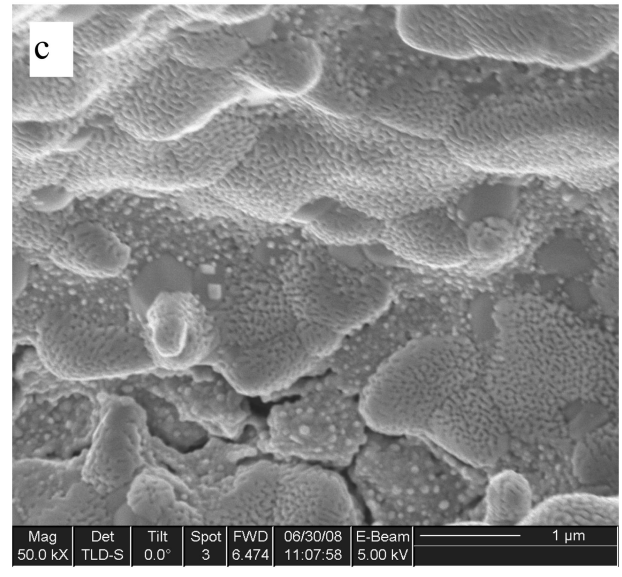

Figure 9. Scanning electron micrograph of $La_{0.33}Sr_{0.67}Ti_{0.92}Mn_{0.08}O_{3\pm\delta}$−YSZ (Ti/Mn = 11) composites after reduction in humidified (3% H_2O) H_2 at 800 °C for more than 100 h, with different initial sintering temperatures: (a) 1100 °C, (b) 1200 °C, and (c) 1300 °C.

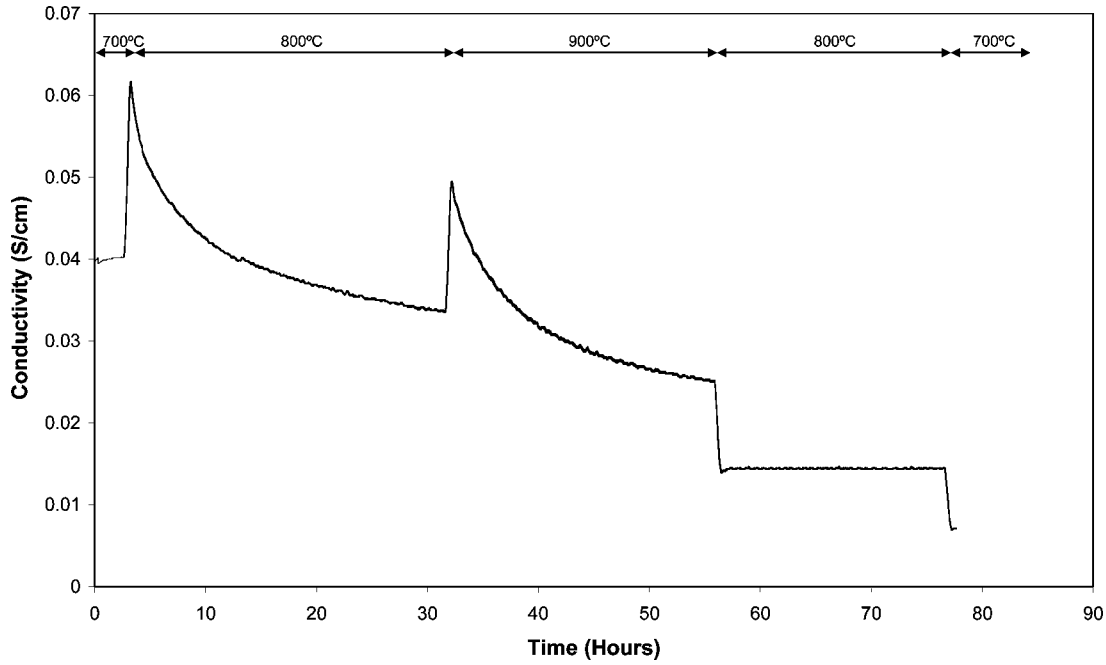

Figure 10. Evolution with time of the conductivity of a LSTM-YSZ (Ti/Mn = 0.5) composite during a thermal cycle in humidified H_2.

$La_{0.33}Sr_{0.67}Ti_{0.33}Mn_{0.67}O_{3\pm\delta}$−YSZ (Ti/Mn = 0.5) composites. The LSTM oxides thus form a similar coating layer over the YSZ, as was previously described for LSCM. To demonstrate the presence of this coating layer, the image has been purposely taken on a cracked surface. The fact that the YSZ grain boundaries remain apparent shows that a thin coating has been deposited. The YSZ wetting is particularly interesting for the composition featuring a high Ti content, since LST compounds do not form a coating over the YSZ surface,[28] as shown on Figure 7b. Therefore, the wetting of the YSZ by the oxide can be attributed to the presence of Mn on the B-site of the ABO_3 structure.

Figure 8 shows the evolution of LSTM films in fuel conditions for the three Ti/Mn ratios described above. SEM images were taken after the structures had been annealed for several hours in humidified H_2 at 800 °C. The LSTM dense film breaks up into interconnected nanoparticles for each composition, but differences can be observed according to the Ti/Mn ratio. In Figure 8a (Ti/Mn = 2), two different morphologies can be seen on the LSTM film: a fine nanoparticulate layer visible in the bottom of the picture and a coarser LSTM structure visible in the upper part of the picture. Examination of the micrograph shows that the coarser structure is mainly located on the concave zones of the YSZ surface, while the finer structure is confined to more convex surfaces. This suggests that this phenomenon might be due to some unevenness in the deposition process, which is driven by capillary action, leading to thinner films on convex surfaces and thicker films in concave areas. To some extent, this phenomenon is apparent in all the micrographs shown in Figure 8 (Ti/Mn = 1 in Figure 8b and Ti/Mn = 0.5 in Figure 8c) but is certainly less apparent as the Mn content increases. This again shows/suggests that the Mn content has a significant effect on the characteristics of the evolved microstructure. The more Mn is present on the B site of the ABO_3 structure, the closer to a thin particulate coating the structure will get.

The temperature at which the LSTM phase is formed has been studied in more detail for composites showing a high Ti content, Ti/Mn = 11. Figure 9 shows images of the structures corresponding to different initial sintering temperature of the oxide phase, after more than 100 h of reduction in humidified H_2 at 800 °C. For 1100 °C (Figure 9a), the structure morphology is close to a LST-YSZ composite one, with no wetting of the YSZ surface. At higher firing temperatures, wetting of the YSZ phase is obtained. Zones of coarsening are more apparent for 1200 °C (Figure 9b) than for 1300 °C (Figure 9c). This shows that a higher temperature shows that a higher initial firing temperature can also facilitate a thin wetted coating layer on the YSZ surface, which in turn leads to a finer particulate structure on reduction. These results demonstrate that only a small amount of Mn (8%) on the B-site of the ABO_3 structure, along with a high enough sintering temperature, is sufficient to obtain wetting of the YSZ surface.

Conductivity tests have also been carried out on LSTM composites. LSTM impregnated YSZ composites have undergone a thermal cycle in humidified H_2, from 700 to 900 °C. Figure 10 illustrates the conductivity evolution as a function of time during the thermal cycle for Ti/Mn = 2. A conductivity decrease, following a similar trend to the one observed for LSCM (Figure 3), can be seen at both 800 and 900 °C. As for LSCM, the diffraction patterns taken after the experiments show no discernible change in structure/phase composition. This conductivity decrease can therefore be assigned to the microstructural reorganization. Once the film evolution process is completed at 900 °C, conductivities are stable when the temperature is decreased. The same behavior was observed for Ti/Mn =1.

Discussion

We see interfacial interactions between impregnated and framework oxides reminiscent of wetting behavior of liquids

on solid surfaces. The strongest interactions with zirconia are for Mn-rich perovskites. We suggest that this either relates to the interaction of Mn in perovskite with the surface or to volumetric changes of the perovskite on reduction. As the increase in unit cell volume of LSCM on reduction is at most 1%[30] and the structure that remains is cubic for both oxidized and reduced forms at these temperatures,[31] we do not consider that structural changes are sufficient to drive these morphological changes. As wetting is much reduced under fuel conditions, with the perovskite dewetting and forming small grains, it seems that reduction of Mn from 3+ to 2+ dramatically changes the interaction between the LSCM film and YSZ. For LSCM it is well documented that the average oxidation state of Mn changes from ~3.5+ to ~2.5+ on changing from oxidizing to fuel conditions at 800 °C.[32] Investigations of Mn solubility in zirconias[33,34] clearly show that Mn II is more soluble in cubic YSZ than Mn III or Mn IV, and it is suggested that this relates to the better suitability of the Mn II electronic configuration to the cubic 8-fold coordination associated with cubic fluorite structure. It therefore seems most likely that the solubility of the lower oxidation state Mn in the cubic YSZ weakens the interfacial interaction, possibly by decreasing the Mn concentration at the interface, allowing the Mn containing perovskites to reorganize into nanoscale particles.

(31) Tao, S. W.; Irvine, J. T. S. *Chem. Mater.* **2006**, *18*, 545–35460.
(32) Plint, S. M.; Connor, P. A.; Tao, S.; Irvine, J. T. S. *Solid State Ionics* **2006**, *177*, 2005.
(33) Chen, M.; Hallstedt, B.; Gauckler, L. J. *Solid State Ionics* **2005**, *176*, 1457.
(34) Occhiuzzi, M.; Cordischi, D.; Dragone, R. *Phys. Chem. Chem. Phys.* **2003**, *5*, 4938.

Conclusion

The interaction between impregnated oxides and their host framework has been found to drive new interfacial structures that are sensitive to thermal and redox conditions and history. An important new tool is illustrated to control and optimize the interfaces of important electrochemical systems such as solid oxide fuel cells.

Acknowledgment. We thank the U.S. Office of Naval Research for support for this collaboration. G.C. and J.T.S.I. also thank EPSRC for support through, Senior Fellowship, Carbon Vision and Supergen schemes. We also thank to thank Stewart McCracken of MCS Ltd., Edinburgh, for assistance with SEM studies.

CM803149V